THE ASTROPHYSICAL JOURNAL, 480:840–849, 1997 May 10
© 1997. The American Astronomical Society. All rights reserved. Printed in U.S.A.

CONTRIBUTION OF LOW-l p MODES TO THE SOLAR EQUATORIAL ROTATION PROFILE

M. C. RABELLO SOARES, T. ROCA CORTÉS, AND A. JIMÉNEZ
Instituto de Astrofísica de Canarias, E-38205 La Laguna, Tenerife, Spain

T. APPOURCHAUX
Space Science Department of ESA, ESTEC, NL-2200 AG Noordwijk, The Netherlands

AND

A. EFF-DARWICH
Instituto de Astrofísica de Canarias, E-38205 La Laguna, Tenerife, Spain
Received 1996 August 28; accepted 1996 December 5

ABSTRACT

The solar equatorial velocity profile is known down to the base of the convection zone with high precision ($\leq 1\%$); from here downward until approximately 0.5 $R_\odot$, it seems to be constant, independent of latitude, and lower than the equatorial surface rate. This result comes from the inversion of high-l p-mode observations (Thompson et al. 1996), while low-l p modes, which penetrate deeper, are not measured to the precision required. Recently, new results from the LOWL instrument on such modes suggest that deeper down, the rotation rate could be even slower (Tomczyk, Schou, & Thompson 1995a). Here results from LOI-T, a low-resolution high-precision photometer, are presented and analyzed to yield accurate measurements of the frequencies and splittings of modes with $2 \leq l \leq 8$. The accuracy of the frequency determinations and the agreement with the best results yielded by low- and high-l instruments give credit to the results and show its capability as an intercalibrating tool for experiment. The splittings found, combined with those of GONG (high-l modes), are used to perform an inversion of the equatorial rotation profile in the radiative interior; the result found is that the region from $0.2 \leq r/R_\odot \leq 0.4$ rotates slower than the surface rate.

Subject headings: Sun: interior — Sun: oscillations — Sun: rotation

1. INTRODUCTION

In the latest two decades, the ability to measure the solar interior structure and dynamics using helioseismic techniques has already been proved. The discovery of very low l p modes (Claverie et al. 1979; Grec, Fossat, & Pomerantz 1980) that penetrate down to the solar core and of very high l values (Deubner 1975; Duvall & Harvey 1983) opened this field of research. Discoveries made by many authors have followed, using very different techniques, which achieved very accurate frequency measurements (better than 30 parts per million [ppm]) of p modes, mainly from 2 to 4.5 mHz. These frequencies have also been inverted to yield the internal structure of the Sun and its rotation.

In particular, the first evidence for subsurface solar rotation came from high-degree mode observations (Deubner, Ulrich, & Rhodes 1979) that showed how the rotation rate was slightly increasing beneath the photosphere. Soon after, Duvall & Harvey (1984) measured the frequencies of sectorial modes with l up to about 100, which gave for the first time the possibility to make an inversion to obtain the profile of the solar equatorial velocity (Duvall et al. 1984). In the meantime, Claverie et al. (1981) measured the first rotational splittings, although averaged over several n values, of p modes with $l = 1$ and 2. Even though the results of Duvall & Harvey (1984) were inaccurate, at these low-l values, both results were compatible. Later, many measurements of high–l-value modes were made (e.g., Brown 1985; Libbrecht 1989) that have given rise to solar rotation profiles, both in radius and latitude, below the base of the convection zone, down to 0.4 $R_\odot$ (see Libbrecht & Morrow 1991).

On the other hand, for very low l-value modes, it is much more difficult to measure the splitting, for three main reasons: first, the measured lifetime of the modes is, at most, as long as one rotational period; second, the rotational period is far larger than the period of the modes; and third, there are fewer components in the multiplets to measure. These explain the nonconcordant results for the $l = 1$ splitting, measured in the past by several researchers (Pallé et al. 1988; Toutain & Fröhlich 1992; Loudagh et al. 1993). As a matter of fact, the scenario nowadays shows a wide variety of results for these splittings, whose scatter is larger than quoted observational errors. Although there might be some possibility that such splitting could change with the solar activity cycle (Jiménez et al. 1994), which may, at least partially, explain the scatter, the latest results seem to converge toward a rather slow value of these splittings (Lazrek et al. 1996)—so low that it could even imply a core rotating significantly slower than the surface (Elsworth et al. 1995).

In the frequency measurements of the p modes, there is a gap in the possible values of l, for which frequencies are not so well determined. Disk-integrated sunlight instruments, at ground level, can only detect p modes of l up to 4, provided that the signal is integrated for long enough (roughly 1 continuous year; see Chaplin et al. 1995); further than this value, the signal is below the noise level that prevents its detection. At the other end, until very recently, high-resolution instruments (both spectrometers and photometers) were not stable enough to detect reliably mode frequencies and/or splittings of modes with l values below about 6 or so.

The LOWL instrument (Tomczyk et al. 1995b) is a magneto-optical filter with enough stability to measure modes with $1 \leq l \leq 80$. The inversion of such a coherent

data set provides probably the best up-to-date rotational profile. Moreover, a low-resolution Sun photometer, LOI-T, has been operational since mid-1994; this is the qualification model from the LOI, an instrument that is part of the VIRGO experiment on board SOHO (Andersen et al. 1988). A preliminary analysis of its results (Appourchaux et al. 1995a, 1995c) demonstrated its capability in detecting p modes with l up to 6, even at ground level, measuring its frequencies and first splitting coefficients. Both experiments are very stable and yield good data; moreover, they are also of importance because they are able to intercalibrate older experiments that only measured either very low l or high-l p modes, providing a means of measuring systematic errors that are very important in understanding the discrepancies between the various data sets; they could also be used to intercalibrate space experiments (by comparison with LOI), on board SOHO, and ground-based networks, such as GONG, IRIS, and BISON.

Here, the results of a thorough analysis of ground-based LOI-T data are presented. The method of analysis allowed us to measure more than twice the number of multiplet frequencies as before, with $2 \leq l \leq 8$, and the splitting coefficients for each multiplet. These measurements are compared with the results of a preliminary analysis of LOI-T data. Furthermore, they are compared with results of integral sunlight measurements (MARKI, at Observatorio del Teide), with those from moderate spatial resolution (LOWL, at Mauna Loa), and with the later results from GONG. Finally, these measurements, complemented with the ones from GONG, are inverted to yield the equatorial solar velocity that will extend deeper than 0.4 $R_\odot$.

2. INSTRUMENT AND OBSERVATIONS

The LOI instrument is a low-resolution photometer to observe the Sun based on an original idea and design by Andersen et al. (1988). The instrument has been already described in detail elsewhere (Appourchaux et al. 1995b). Briefly, it consists of a Ritchey-Chrétien telescope ($f = 1300$ mm) imaging the Sun through a 5 nm passband interference filter centered at 500 nm. The detector is made out of 12 scientific pixels surrounded by 4 guiding ones (see Fig. 1). The shapes of the scientific pixels are trimmed to detect low-degree oscillation modes ($l < 10$; see Appourchaux & Andersen 1990). The guiding pixels are four quadrants of an annulus with an inner and outer radius of about 0.95 and 1.05 solar radius, respectively. The telescope secondary mirror is controlled by two orthogonally placed piezoelectric stacks, allowing the image to be stabilized in a closed servo loop with a 10 Hz bandwidth; its total range is $\pm 5'$ with a $0''.2$ precision. The electric current of each scientific pixel is amplified and digitized using voltage-to-frequency converters (VFCs), and the current of each guiding pixel is amplified and digitized using analog-to-digital (A/D) converters. The 12 scientific pixels are read simultaneously, while the 4 guiding ones are read sequentially. The sampling time of the instrument is approximately 13.42 s, of which about 99% is integration time, provided by a well-stabilized high-precision oscillator. This instrument is a part of the VIRGO experiment on board SOHO (Fröhlich et al. 1995).

In order to test it on the ground, its qualification model was installed on an equatorial mount on 1994 May 2 at Observatorio del Teide (Tenerife). It is named LOI-T, and

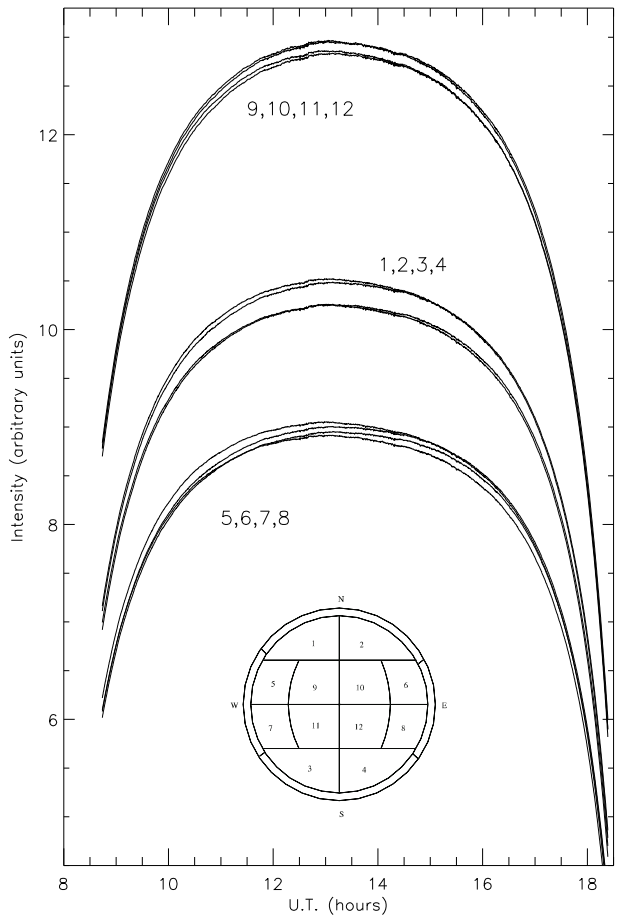

FIG. 1.—(*a*) LOI-T detector configuration showing the approximate shape of the pixels and (*b*) scientific raw data showing Earth's atmospheric extinction effect on the radiance over each pixel for a typical day: 1993 February 23.

since then, it has been working continuously. No instrumental changes have been made in any of the parts of the photometer other than the inclusion of an external PC to control data acquisition. This computer also provides the absolute timing from its internal clock that is calibrated every day against a standard global positioning satellite (GPS) signal. Housekeeping parameters, such as temperatures on detectors and amplifiers, guiding pixel signals, voltages on the piezoelectric stacks, etc., are also recorded to assess instrumental performance. The observations that will be analyzed here start on 1994 May 12 and end on 1995 July 17. The scientific raw data from a typical day are shown in Figure 1.

Before analyzing the scientific data, the first step consists in a "cleaning process," in which points, because of bad weather conditions and/or instrument failures, are omitted; also, data taken 5 hr away from local noon were not considered, as they strongly suffered from differential atmospheric extinction. In a second step, we checked the guiding pixel's signals in order to be sure that the guiding worked perfectly—in other words, that each pixel collected the light from the part of the Sun that is expected. When the differences between the signals, from north and south pixels or between the east and west ones, were out by more than 5 σ, the data were also excluded.

3. DATA ANALYSIS

The procedure for data reduction and analysis that

follows here has been developed independently by Rabello Soares (1996), following earlier indications found in Appourchaux & Anderson (1990); this implies that it might be different in many details from earlier data reductions (Appourchaux et al. 1995a, 1995c). The procedure starts by correcting for Earth's atmospheric extinction. Therefore, a new signal is defined: from the measurement of each pixel, an average of all 12 pixel measurements is subtracted and, further, divided by it:

$$R_j = \frac{I_j - [\sum_{j=1}^{12} I_j]/12}{[\sum_{j=1}^{12} I_j]/12}, \quad (1)$$

where I_j is the signal measured for pixel j ($j = 1$ to 12). As the fluctuations of the atmospheric transparency have a higher spatial coherence than the pixel area on the detector and these are read simultaneously, this is a very efficient method for suppressing the effect of Earth's atmospheric noise (Appourchaux et al. 1995c; Rabello Soares et al. 1996). However, a very low frequency trend (~ 12 hr period) due to differential atmospheric extinction is still present. Thus, a slow "moving mean" filter has been applied to the residuals to smooth out variations longer than about 20 minutes. Furthermore, the standard deviation of the residuals (σ) for each pixel was calculated, and points whose values are out by more than $\pm 5\ \sigma$ in any of them were replaced by zeros in all pixel series.

Finally, the whole data set was divided into two series, each 216 days long. In it, each day has been weighted by the inverse of the daily variance of its residuals relative to their minimum of all observed days, as a measure of quality, to give more weight to the best days. Obviously, this changes the window function that is later taken into account when calculating the power spectrum; the reward is an improvement in the signal-to-noise (S/N) ratio in the frequency band of interest. The final duty cycle achieved is about 25%. These are the residuals, $p_k(t)$, with $k = 1, \ldots, 12$ pixels, that will later be used for harmonic analysis to detect p modes. The results for a typical day are shown in Figure 2, for three representative pixels only.

As the LOI detector has some spatial resolution, it is very difficult to make the mode identification without using any filter that isolates a given individual mode. Appourchaux & Andersen (1990) developed a method due to Christensen-Dalsgaard (1984), in which an optimal linear combination of the pixels selects a given (l_0, m_0) mode. The proposed optimal weights $q_j(l_0, m_0)$ are those that minimize the following quantity:

$$\sum_{l=0}^{l_{\max}} \sum_{m=-l}^{+l} [1 - \delta(l, l_0)\delta(m, m_0)] \left| \sum_{j=1}^{12} q_j(l_0, m_0) U_j(l, m) \right|^2, \quad (2)$$

where δ is the Kronecker delta, l is the degree of the mode, m is its azimuthal order, $l_{\max}$ is the degree limit set by the resolution of the detector and the S/N ratio of the data, and $U_j(l, m)$ is the complex spatial response function defined by

$$U_j(l, m) = \int_{A_j} I(\sin\theta \cos\phi) P_l^m(\cos\theta) e^{im\phi} \times \sin^2\theta \cos\phi \, d\theta \, d\phi, \quad (3)$$

where (θ, ϕ) are the usual spherical coordinates, A_j is the integration domain defined by the actual geometry of the pixel j, $P_l^m(\cos\theta)$ are the Legendre polynomials, and $I(\sin\theta \cos\phi)$ is the limb-darkening function.

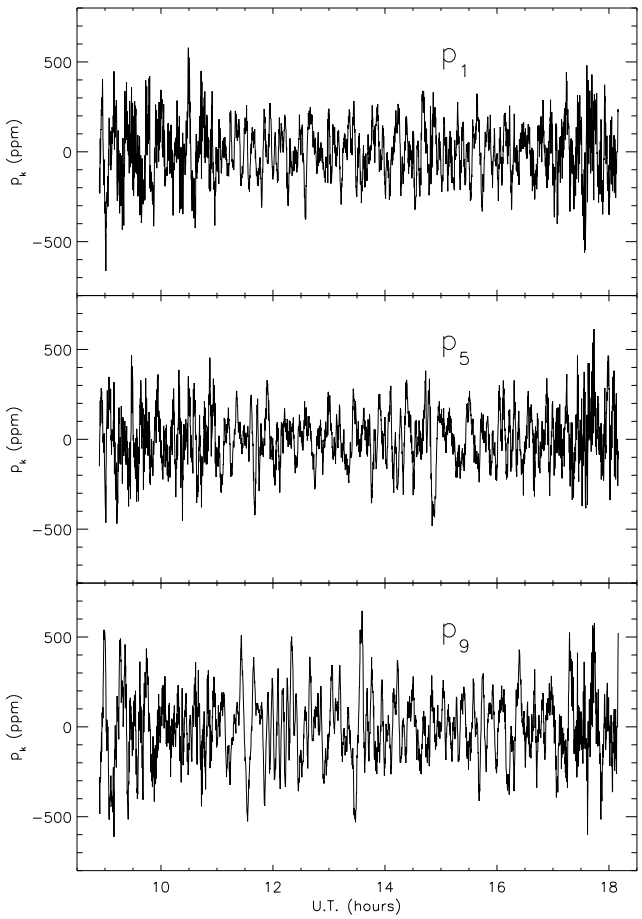

FIG. 2.—Radiance ratio R_j for three representative pixels after the reduction procedure has been applied (see text) on the same day cited in Fig. 1. Vertical scale is in ppm and is the same for the three plots, which have been shifted only vertically for clarity: (*a*) p_9, one of the central pixels; (*b*) p_5, one of the east-west pixels; and (*c*) p_1, one of the north-south pixels.

Following this method we have computed the optimal weights to be applied to each pixel to select a given oscillation mode (l, m). However, several important points have to be taken into account in the whole procedure to obtain unbiased and precise results. First, as pointed out by Appourchaux et al. (1995a), the correct orientation of the solar disk onto the detector has to be correctly determined. In this work, it has been done experimentally and independently of earlier data reductions (Appourchaux et al. 1995a, 1995c).

Second, the size of the pixels and their actual shape have been accurately computed. This determines the correct integration limits A_j of the spatial response function $U_j(l, m)$ associated with the optimal weights of each pixel and all the computations derived from them. In addition, the determination of the minimum $l_{\max}$ compatible with the noise present in the spectra has been studied. All of these calculations have been done accurately to the appropriate numerical precision.

Third, the size of the solar image, which depends on the Sun-Earth distance, changes with time along the year, varying also the integration limits of the pixels in the detector; therefore, the optimal weights have been computed for each day taking into account this effect.

Fourth, one has to take into account the Sun's apparent precession of the solar rotation axis along the year, which changes the part of the solar disk measured by each pixel. A correction is calculated for every day, which depends on the angles P and B_0, by means of the appropriate rotation matrix applied to the spatial response function $U_j(l, m)$, following Edmonds (1960). For some coefficients of the optimal weights, the variation along the year is very slow, and even interpolation of weekly averaged values could be used; but for others, a change of up to 50% per day has been found, especially when degree l increases.

These optimal filters (or weights) are complex, in general; they have many properties on top of the one of isolating a given (l_0, m_0) mode: for instance, the complex conjugate of an optimal filter for $(l_0, +m_0)$ gives the optimal filter for $(l_0, -m_0)$, therefore allowing the separation, in the frequency domain, of the $+m_0$ from the $-m_0$ modes. For a detailed account, see Appourchaux & Andersen (1990).

Once the optimal weights for each day and for a given (l_0, m_0) mode have been computed, a time series is built by performing the following linear combination of the pixel signals:

$$I_{l_0,m_0}(t) = \sum_{d=1}^{M} \left[\sum_{k=1}^{12} q^R_{k,d}(l_0, m_0) p_{k,d}(t) + \imath \sum_{k=1}^{12} q^I_{k,d}(l_0, m_0) p_{k,d}(t) \right], \quad (4)$$

where q^R_k and q^I_k are the real and imaginary parts, respectively, of the optimal filter for the given (l_0, m_0) mode at a given day d, and M is the length of the series in days. In doing so, we obtain a time series in which all (l, m) modes but the (l_0, m_0) are severely attenuated. However, they are not perfect, and some modes are not attenuated as much as one would want; they are spurious modes, forming the so-called cross talk, which will be discussed later.

4. ANALYSIS IN THE FREQUENCY DOMAIN

After filling the gaps of the series with zeroes, the power spectra of the complex time series, for each (l, m) mode and for each of the two observing series, have been calculated, and the average of these two is the basis of the subsequent analysis. The resulting frequency resolution is 54 nHz. Figure 3 shows in an (m-ν) diagram the power spectra for modes $(n = 20, l = 2)$ and $(n = 18, l = 6)$. Note the first-order sidebands, due to the day-night observing cycle, and the different S/N ratio for both plots. In the case of $l = 6$ the signal power is lower because of the lower sensitivity of the detector, and the noise seems higher because of an increase of the cross talk with other, incompletely filtered, modes.

The data reduction procedure, through the definition of the signal R_j (eq. [1]), although nicely correcting for atmospheric extinction, has the disadvantage of preventing the detection of the $l = 0$ mode. Moreover, the $l = 1$ modes are also severely attenuated to a very low S/N ratio level, which also ruined the measurement of these rather important modes.

The first step in the measurement of the frequencies of the peaks present in the spectra consists of fitting appropriate functions to them. As a stochastic nature for the excitation of solar p modes is assumed, their profile will be a Lorentzian. To start with, we have fitted, at intervals of 30 μHz (in the case of $l \leq 6$) around the frequency of a given (n, l, m) mode, a sum of 3 Lorentzian profiles (the main peak and its first-order sidebands); for $l = 7$ and 8, intervals of 36 μHz were used. The fitting method used is a maximum likelihood technique (Anderson, Duvall, & Jefferies 1990, Appourchaux et al. 1995c). Once the fit converges for each mode, the value of the following parameters are obtained: height of the peak (related to the mean amplitude of the mode), width at half-amplitude (Γ, related to its lifetime), frequency of the central peak, and background noise level.

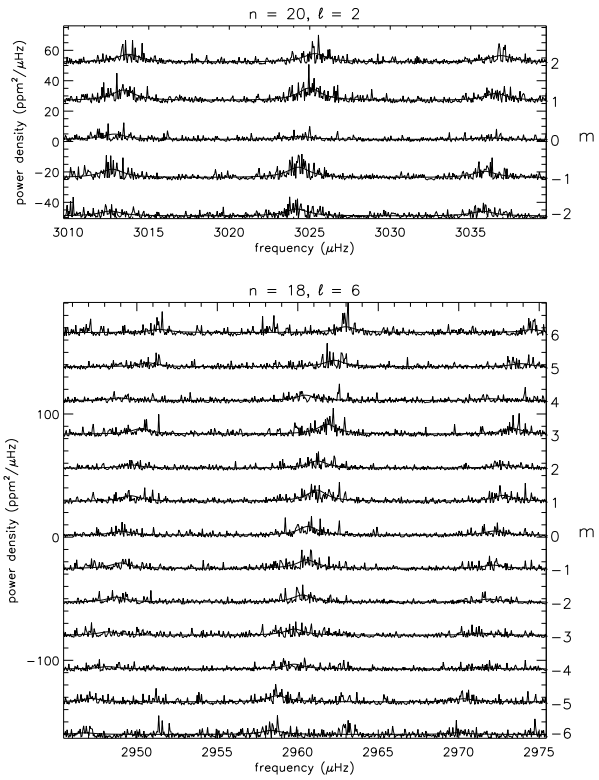

FIG. 3.—Power density spectra for the modes: up for multiplet (16, 2) and down for (16, 6). Only $m = 0$ in each case is drawn to scale; other m values have been appropriately shifted in vertical scale for clarity. Bold lines show the best fit to the above-mentioned peaks and its sidebands (see text). Also notice the presence of other peaks, e.g., in the $m = \pm 6$ modes, in the spectra as a consequence of nonzero cross talk among the modes.

Following this first fit, the obtained values of Γ for each (n, l, m) mode was averaged over m and plotted against order n, for each degree l. A straight line was fitted to them (enough for the frequency interval used) and the variation of Γ with n was empirically obtained. Now, keeping fixed the values for Γ obtained from these fits, each spectrum was fitted again. This allowed faster and better fits with a better determination of the frequencies and amplitudes. Figure 3 also shows, in bold line, the Lorentzian profiles obtained for a given (n, l, m) mode.

This procedure provided good determinations of the frequencies of many (n, l, m) modes. In Figure 4, for each l value, the relative values of these frequencies to the central frequency of each multiplet, averaged over n, are plotted against m. This shows how frequencies of a given multiplet vary with azimuthal order. However, one must pay attention to the presence of cross talk peaks in the spectra that may influence the fits only to individual (n, l, m) modes; on the other hand, the fact that each (n, l) multiplet splits into $(2l + 1)$ components with different m values because of rotation in a known way could also be used in the fits of the spectra by, e.g., simultaneously fitting a whole multiplet

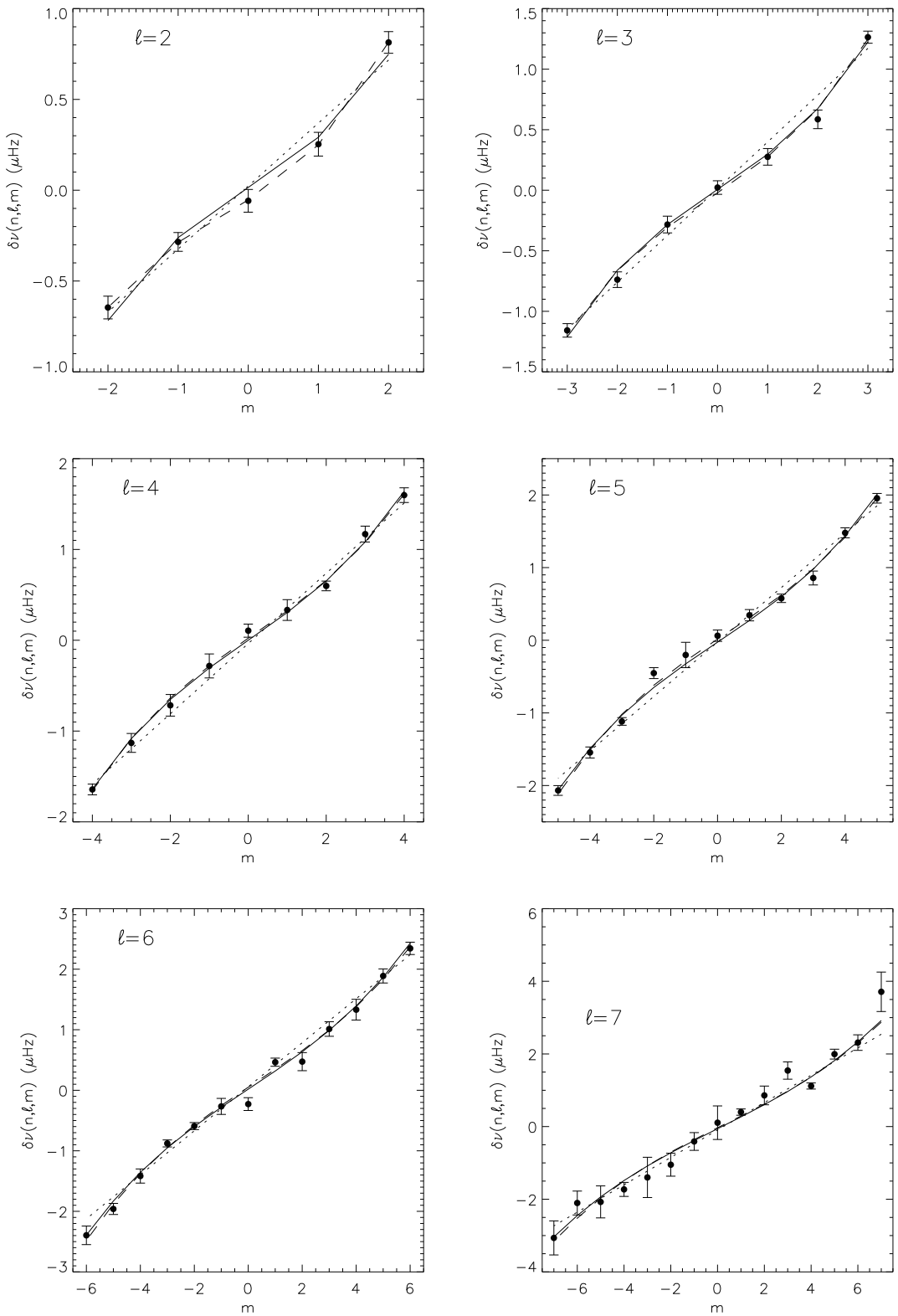

FIG. 4.—For a given l value, we show the frequency difference between each peak and the mean of them, as a function of m, averaged over the measured n values. Dotted lines are the best linear fits, dashed lines are the best fits to eq. (6), and full lines are the best fits to the same equation, but taking into account only odd coefficients.

structure, as will be shown in the next paragraph. The results of the fit procedure just described will illustrate the splitting process induced by rotation and also provide frequency determinations that are useful for comparing results and as better first guesses for the multiplet fit that we will describe next.

5. FREQUENCIES AND SPLITTING MEASUREMENTS OF MULTIPLETS

Axisymmetric perturbations to spherical symmetry, such as the solar internal differential rotation, remove the degeneracy of frequencies of the modes with the same l and n but

TABLE 1

FREQUENCIES AND SPLITTING ODD COEFFICIENTS

	$l = 2$			$l = 3$			$l = 4$			$l = 5$		
n	ν	a_1	a_3	ν	a_1	a_3	ν	a_1	a_3	ν	a_1	a_3
13.....	2085.77 ± 0.16	...	...	2137.43 ± 0.10	...	...	2186.39 ± 0.09	...	...	2235.34 ± 0.07	362 ± 45.	178 ± ...
14.....	2221.75 ± 0.10	...	...	2273.35 ± 0.10	...	...	2324.13 ± 0.07	417 ± 30	−72 ± ...	2370.02 ± 0.12	...	...
15.....	2352.47 ± 0.09	...	...	2407.81 ± 0.08	...	...	2458.73 ± 0.08	380 ± 41	−89 ± ...	2506.20 ± 0.07	424 ± 36	84 ± 44
16.....	2485.87 ± 0.11	432 ± 57	129 ± 144	2541.59 ± 0.09	413 ± 36	75 ± 87	2593.12 ± 0.07	379 ± 23	−22 ± 41	2641.24 ± 0.06	391 ± 21	26 ± 35
17.....	2619.72 ± 0.11	454 ± 98	−79 ± 112	2676.21 ± 0.06	433 ± 28	−57 ± 50	2728.57 ± 0.05	434 ± 18	−19 ± 32	2777.25 ± 0.05	418 ± 16	70 ± 26
18.....	2754.34 ± 0.07	...	...	2811.44 ± 0.04	390 ± 20	90 ± 37	2864.20 ± 0.05	427 ± 16	27 ± 31	2913.66 ± 0.05	426 ± 14	3 ± 24
19.....	2889.53 ± 0.05	420 ± 49	158 ± 89	2946.98 ± 0.05	476 ± 23	106 ± 44	3000.22 ± 0.04	465 ± 13	1 ± 25	3049.91 ± 0.05	401 ± 14	41 ± 22
20.....	3024.67 ± 0.06	...	...	3082.34 ± 0.05	375 ± 30	120 ± 52	3135.92 ± 0.05	409 ± 16	85 ± 29	3186.20 ± 0.04	407 ± 16	62 ± 27
21.....	3159.80 ± 0.07	472 ± 53	...	3217.87 ± 0.06	409 ± 28	65 ± 57	3271.66 ± 0.05	387 ± 22	47 ± 42	3322.72 ± 0.07	432 ± 27	25 ± 38
22.....	3295.08 ± 0.09	556 ± 103	6 ± 143	3353.58 ± 0.08	452 ± 36	−42 ± 63	3407.86 ± 0.06	...	...	3460.69 ± 0.02	...	...
23.....	3430.62 ± 0.12	441 ± 74	51 ± 176	3489.67 ± 0.13	464 ± 89	112 ± 115	...	...	...	3601.62 ± ...	...	...
24.....	3566.86 ± 0.20	...	...	3626.48 ± 0.18	463 ± 75	446 ± 141	3680.27 ± 0.12	...	...	3733.09 ± 0.30	...	...
25.....	3703.24 ± 0.43	...	...	3760.47 ± 0.31	...	...	3818.79 ± ...	...	...	3870.44 ± 0.24	...	...

	$l = 6$			$l = 7$			$l = 8$		
n	ν	a_1	a_3	ν	a_1	a_3	ν	a_1	a_3
13.....	2279.89 ± 0.05	...	...	...	...	...	...	...	...
14.....	2416.67 ± 0.14	422 ± 42	263 ± ...	...	...	...	...	...	...
15.....	2551.15 ± 0.10	418 ± 29	−53 ± 50	2594.12 ± 0.17	...	...	2634.82 ± 0.06	...	...
16.....	2687.11 ± 0.05	376 ± 15	104 ± 21	2731.04 ± 0.11	379 ± 30	43 ± 41	2774.51 ± 0.15	...	...
17.....	2823.74 ± 0.05	413 ± 12	31 ± 19	2868.28 ± 0.07	464 ± 15	−56 ± 25	2912.00 ± 0.12	451 ± 21	−12 ± 46
18.....	2960.69 ± 0.04	415 ± 12	5 ± 19	3005.54 ± 0.07	473 ± 15	39 ± 26	3049.42 ± 0.14	...	...
19.....	3097.23 ± 0.05	412 ± 17	19 ± 26	3142.81 ± 0.06	431 ± 11	31 ± 22	3186.13 ± 0.17	...	...
20.....	3233.96 ± 0.06	445 ± 15	−33 ± 22	3280.07 ± 0.08	421 ± 16	−37 ± 28	3320.62 ± 0.58	...	...
21.....	3370.90 ± 0.07	436 ± 24	28 ± ...	3418.68 ± 0.08	...	...	...	...	...
22.....	3508.45 ± 0.10	...	...	3554.87 ± 0.18	...	...	...	...	...
23.....	3646.27 ± 0.43	...	...	3691.90 ± 0.16	...	...	...	...	...
24.....	3783.52 ± ...	...	...	...	...	...	...	...	...
25.....	...	...	...	...	...	...	...	...	...

NOTE.—Frequencies, in μHz, and splitting odd coefficients (a_1 and a_3; see text) in nHz, with their errors found by fitting each multiplet taking into account the *cross talk*.

different azimuthal order m. If the solar rotation frequency were only a function of radius $\Omega(r)$, then the variation of frequency with azimuthal order m (as seen from a sidereal frame) would be given by the following:

$$\delta\nu_{nlm} = \nu_{nlm} - \langle\nu_{nl}\rangle = m\,\frac{\bar{\Omega}}{2\pi}\,, \tag{5}$$

where $\langle\nu_{nl}\rangle$ is the frequency averaged over m, and $\bar{\Omega}$ is an appropriate average of $\Omega(r)$ over the depth range sampled by the modes. The result of a linear fitting to the above measured frequencies, averaged over n and assuming this simplest approximation, is also shown as a dotted line on Figure 4. As it is readily seen, this is not the best fit we can perform.

Solar differential rotation depends also on latitude and, therefore, $\delta\nu_{nlm}$ will also depend on m in a more complicated way. The frequency variation with m can be expressed as follows:

$$\delta\nu_{nlm} = \nu_{nlm} - \langle\nu_{nl}\rangle = L\sum_{j=1}^{j=N} a_j P_j(m/L) \tag{6}$$

(Duvall, Harvey, & Pomerantz 1986), where P_j are the Legendre polynomials of degree j, and $L = [l(l+1)]^{1/2}$. The choice of m/L rather than m/l reduces the dependence of the coefficients a_j with degree l. The dashed line in Figure 4 is the fit assuming equation (6) with $N = 3$. This is a much better fit; however, as we are analyzing low-degree modes ($l < 8$) only, we are not able to determine accurately coefficients higher than a_3.

The frequency perturbations due to slow rotation are always antisymmetric in m (Cuypers 1980; Brown 1986). Changes in the internal temperature or magnetic field could produce frequency shifts that are symmetric in m, as could rotation that is rapid enough for centrifugal effects to become important. The solid line in Figure 4 represents the same fit as before, but without fitting the a_2 coefficient—this means considering only antisymmetric terms in m (a_1 and a_3). As can be seen, the difference between both fits is negligible for all l values except $l = 2$, where it is well within errors; consequently, we drop the use of a_2, as no new information can be obtained from it.

Coming back to the analysis of the spectra obtained, even with the care in computing the filters to isolate the modes, there is power leakage between them. In fact, the amount of mode power of the nonrejected modes is a measure of the so-called cross talk, and it can be calculated as the modulus of the optimized spatial response function as follows:

$$C(l, m, l_0, m_0) = \left|\sum_{j=1}^{12} q_j(l_0, m_0)U_j(l, m)\right|^2 . \tag{7}$$

As the optimal filters $q_j(l_0, m_0)$ change along time, from day to day, the cross talk calculated for each (l_0, m_0) mode also changes. In order to evaluate its importance in a given spectrum, its daily value was averaged in the whole observational period and normalized to the extracted mode:

$$\sum_{k=1}^{M} C_k(l, m, l_0, m_0)\Big/\sum_{k=1}^{M} C_k(l_0, m_0, l_0, m_0)\,, \tag{8}$$

where M is the number of days of observation. Finally, only the spurious nonrejected modes that have power 1 σ above the noise level were considered. As an example, we found that for $l < 7$, there is cross talk only between the several components of a given multiplet, while for $l = 7$ and 8, the effect of the cross talk between different multiplets becomes important too, being influenced mainly by those with $l = 4$ and 5, respectively.

Now, we are ready to fit simultaneously all components, $2l + 1$, of each multiplet (n, l), plus those spurious modes with enough level of cross talk, plus their first-order sidebands; the line widths also have been kept as constant for each multiplet and equal to the values found in § 4. The frequency interval for the fitting was the same as before for $l < 7$, but it has been increased to 40 μHz for $l = 7$ and 8 to include cross talk with $l = 4$ and 5 modes, respectively, and its sidebands. The central frequencies of each multiplet found in this fit are shown in Table 1. Furthermore, the splittings fitted to equation (6) with only odd coefficients are also shown in Table 1. The obtained multiplet frequencies have been compared to the ones found when fitting single modes only (as explained in § 4). The result is that they agree within errors, yielding a weighted mean value for their relative frequency differences of 1.9 ± 2.4 ppm.

To evaluate the effect of the cross talk on the fits, the process of fitting each multiplet has been repeated, but without fitting the cross talk peaks. The relative differences between the multiplet frequencies yield a mean value of 1.6 ± 2.0 ppm, which clearly shows no effect of the cross talk in the central frequency determination of the multiplets. However, the effect on the determination of the first and second splitting coefficients, a_1 and a_3, is somewhat higher: on the first one, the weighted mean value of their relative differences is $-1.9\% \pm 0.3\%$, which would imply that if cross talk is not taken into account, then the fit would yield lower values for a_1, as already suggested in Appourchaux et al. (1995a); the a_3 coefficient has errors that are too big to yield significant conclusions from the comparison, but the weighted mean value for their relative differences is $-34\% \pm 10\%$, pointing toward the same effect as the one found for a_1.

In addition, we have evaluated the effect of keeping the multiplet line widths constant by fitting again the same multiplets with their line width as a fitting parameter (equal for all multiplet components). The result is that the line widths are somewhat higher than those considered (for some lines up to 30%), but the effect on the central frequency determination is negligible (-2.3 ± 2.3 ppm); however, the a_1 splitting coefficient values tend to be smaller by $2.5\% \pm 0.7\%$, which is marginally significant, but this is compensated by an increase in the a_3 coefficient, yielding a negligible overall effect ($0.6\% \pm 0.6\%$). Thus, the consequence here is that the fit of both splitting coefficients compensated the effect of not fitting the line widths.

6. DISCUSSION OF THE RESULTS

The results found here will be first compared with those found in our preliminary analysis (Appourchaux et al. 1995a). We should stress the fact that we have been able to determine the central frequencies of 78 multiplets, as compared to 33, and the first and second splitting coefficients for more than half of them. To quantify the comparison, the case of the central frequencies shows extremely small differences, well within errors; the weighted mean value of the relative frequency differences is 11.1 ± 8.2 ppm. As far as the first splitting coefficient is concerned, the weighted mean value of its relative differences is negligible ($1.0\% \pm 1.9\%$). These tests show the stability of the results against different ways of analyzing the data.

We can also compare our results with those coming from other experiments, obtained by several authors: first, with those of an integral light resonant scattering spectrophotometer, such as MARKI (Anguera Gubau et al. 1992) taken at solar minimum; second, with those of a magneto-optical filter, such as LOWL (Tomczyk, Schou, & Thompson 1995a), analyzing almost coeval observations; and third, with the first results obtained by the GONG network (Hill et al. 1996; Thompson et al. 1996) at the end of our analyzed period. Figure 5 shows the relative frequency differences between the results found by these instruments and the ones presented here.

Anguera Gubau et al. (1992) provide solar minimum frequencies for $0 \leq l \leq 3$ solar p modes. We have compared their results with ours in the frequencies and modes common to both sets. The weighted average of the relative frequency differences is of -74.3 ± 31.7 ppm. These results show that our values are systematically higher by 234 nHz, as can also be seen in Figure 5. This difference is easily explained by the fact that during the period analyzed here, the solar activity cycle was not at the minimum phase yet; therefore, the frequencies of the p modes will be higher by about the measured quantity (Régulo et al. 1994).

The comparison of LOWL results with ours shows a mean value for the relative frequency differences of -7.8 ± 5.1 ppm. The splitting coefficients cannot be compared directly because Tomczyk et al. (1995a) used a Clebsch-Gordon expansion for the splitting (Ritzwoller & Lavely 1991), rather than the Legendre polynomial expansion that we use; although at high l values the two expansions coincide, this is not the case for the l value modes observed here. However, the weighted mean value of the relative differences in $(a_1 + a_3)$ is of $-3.1\% \pm 1.6\%$.

The GONG results (Hill et al. 1996) come from the analysis of three series of 36 days long averaged (1995 August to 1995 December). The number of modes found here in the interval $13 \leq n \leq 24$ and for $2 \leq l \leq 8$ is approximately twice the number of modes in the same interval found by GONG, as could be expected (because GONG has a high spatial resolution detector and is designed to measure intermediate l modes, while the LOI detector has lower spatial resolution and higher stability). Again, the weighted mean of the relative differences for the frequencies is of -22.4 ± 9.4 ppm, which corresponds to absolute differences of -70.1 ± 27.4 nHz. This result (see Fig. 5) suggests that GONG frequencies are systematically lower than ours, confirming the results obtained by Hill et al. (1996) when comparing his results with other experiments. For the sum of the two splitting coefficients $(a_1 + a_3)$, the obtained weighted mean value of their relative differences is $-6.5\% \pm 2.5\%$, which is not significant.

Finally, other parameters, such as the line widths of the modes measured, obtained as a result of the initial fit (§ 4), agree well within those found already by Elsworth et al. (1990) for low-l modes and Libbrecht (1988) for high-l modes. Moreover, the relative amplitudes for the modes found here as a function of frequency, for different l values, also agree with the expectations derived from lower and higher l observations.

In conclusion, we can say that LOI-T findings agree extremely well with instruments with smaller and higher spatial resolution that measure frequencies of lower and

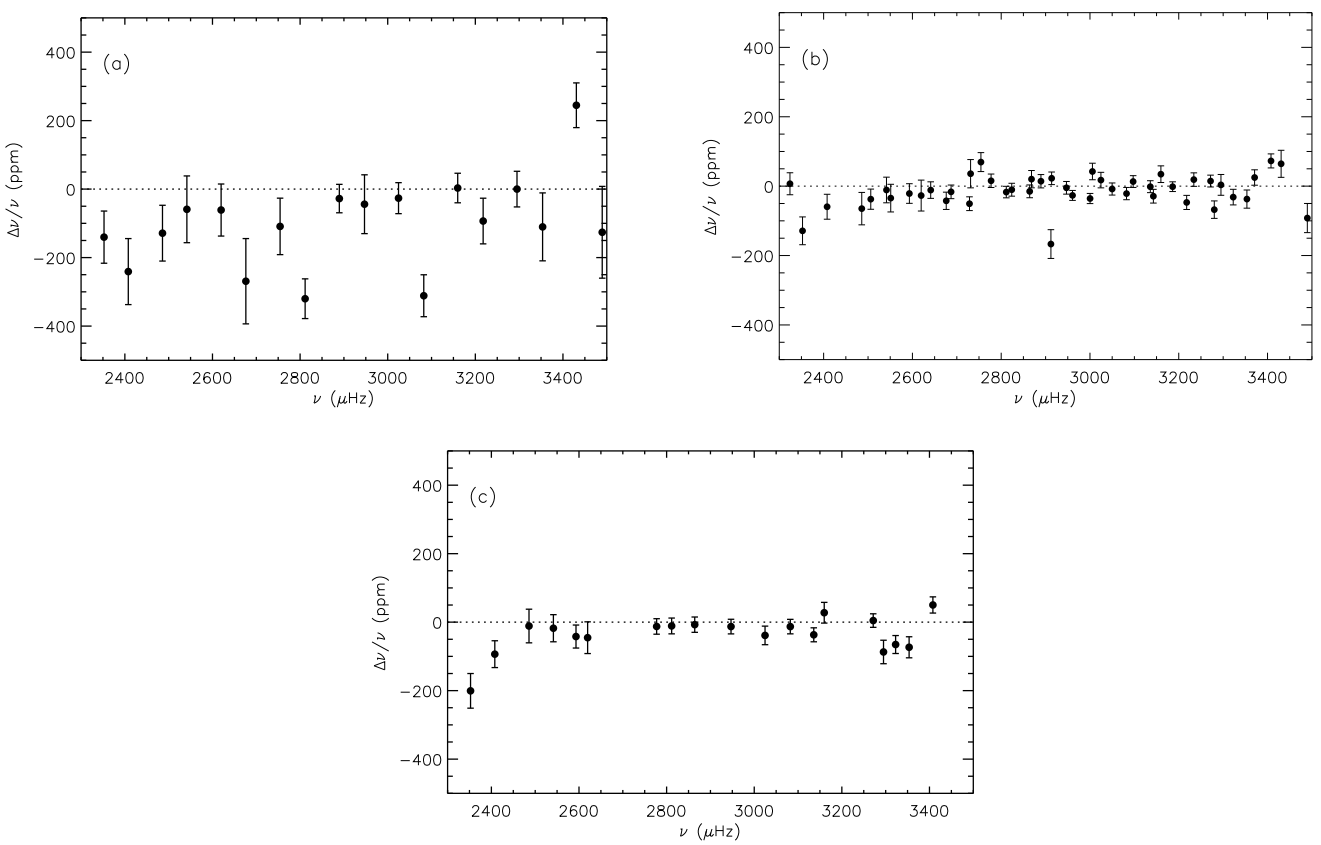

FIG. 5.—Comparison of the multiplets' frequencies found here with those found by other experiments: (*a*) MARKI, (*b*) LOWL, and (*c*) GONG. The relative frequency differences are defined as $(\nu_{\rm inst} - \nu_{\rm LOIT})/\nu_{\rm LOIT}$. The disagreement in the top plot is explained by the change of the frequencies of the modes with solar cycle, while the one at the bottom cannot be explained by the same argument.

higher l-value p modes. This demonstrates its use and capability in filling appropriately the gap in the modes measured by standard instruments. It is expected that data from LOI on board VIRGO will be much cleaner than the LOI-T, and, therefore, it will be possible to measure $l = 0$, 1 and $l \geq 8$ up to probably 15.

7. INVERSION OF THE SPLITTING DATA

Having obtained the splitting coefficients, these are inverted to estimate the Sun's internal rotation rate. The problem of inferring the dependence of the solar rotation on radius and latitude is a two-dimensional problem. However, most inversion methods use so-called 1.5 dimensional inversions, in which the latitudinal dependence is inferred by expanding the measurements of the frequency splittings and the latitudinal dependence of the rotation rate in appropriate polynomials. Morrow (1988) showed how to make linear combinations of the coefficients a_i that reflect the radial variations of angular velocity at any latitude. Unfortunately, this approximation is correct only for high l (Brown et al. 1989), and our data are mainly based on low-l modes. However, inverting only the data obtained here is not useful, because of the errors and the poor sampling along the solar radius. Therefore, we also use the data taken from GONG to round off a set of observations to be inverted. Further, as the sectorial modes are confined to the equator, its splittings can be used to invert the equatorial rotation rate profile. However, sectorial modes with low-l values are not too concentrated toward the equator, as high-l modes are, having some contribution from high latitudes; moreover, as the observed rotation rate below the convection zone is latitude independent, such a contribution will be even lower. Therefore, we are going to study the rotation at the equator using the average of the sectorial modes.

The splitting of sectorial modes can be expressed as follows:

$$\Delta_{nl} = \frac{\delta\nu_{nll} - \delta\nu_{nl-l}}{2l} \approx \frac{1}{2\pi}\int_0^R K_{nl}(r)\Omega(r)dr + \epsilon_{nl}\,, \qquad (9)$$

where Δ_{nl} denotes the measured splittings, ϵ_{nl} denotes their errors, and $K_{nl}(r)$ are the kernels (taken from Gough 1981). The term Δ_{nl} is calculated from the observed a_1 and a_3 splitting coefficients (see eq. [6]) and the errors correspondingly propagated.

Figure 6 shows the results to be inverted Δ_{nl} values, which are closely related to the solar rotation at the equator, as a function of log (ν/L) related to the lower turning point of the mode. The scatter in the values of the splittings for low l is higher than those for high l; this is (partially) due to the fact that the total observed splitting is proportional to m, and as the maximum value of m for a mode is l, the rotational splitting for the low-l modes is not as great as for high-l modes, requiring a higher resolution and better S/N ratio spectra to make the same measurement. To reduce the scatter, we selected the splitting values by locally rejecting in boxes of log $(\nu/L) = 0.2$ those points above 2 σ; this process has rejected around 30% of the points, leaving those plotted in Figure 6. Although it may seems a very restrictive criterion when using a 3 σ rejection criterion instead, the inversion results do not clearly differ (slightly lower below 0.35 $R_\odot$) from those presented here, but they present larger errors.

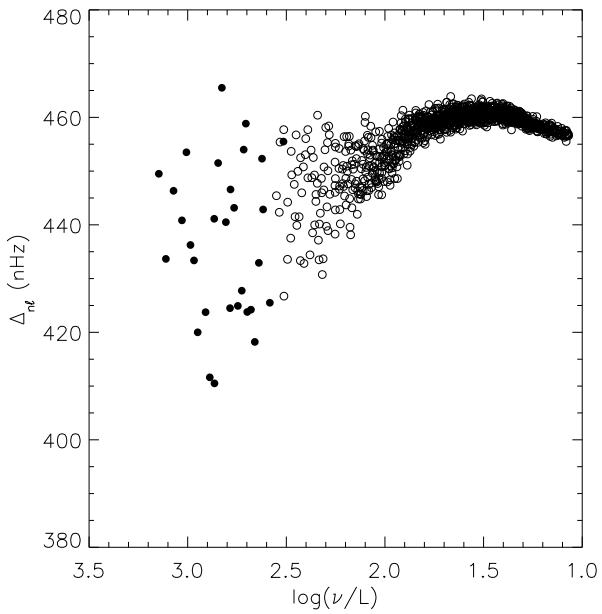

FIG. 6.—Splitting obtained in this work for $2 \leq l \leq 8$ modes (*filled circles*), together with the GONG results for $8 \leq l \leq 140$ modes (*open circles*) (Thompson et al. 1996) as a function of log (ν/L). These are the measured quantities that are inverted.

To invert the above equation, we have used an inversion method developed by Eff-Darwich (1996), named optimal mesh distribution (OMD). This is a hybrid method that uses information from the traditional inversion methods optimal localized averages (OLA) and regularized least squares (RLS). It actually minimizes the following function:

$$\chi^2 = \sum_{nl}\left[\int_0^R \frac{K_{nl}(r)}{\epsilon_{nl}}\,\Omega(r)dr - \Delta_{nl}\right]^2 + \alpha\int_0^R \lambda(r)H(r)dr\,, \qquad (10)$$

where $H(r)$ is a weighting function, $\lambda(r)$ is a smoothing function, and α, the only free parameter of the method, is a proportionality factor whose choice determines the trade-off between depth resolution and noise amplification.

The method (see Eff-Darwich & Pérez-Hernández 1996) looks for an optimal mesh point distribution (improving the computational time problem of OLA), but it solves the inversion problem as in the RLS technique, including, however, a smoothing function weighted differently, depending on the point in the mesh.

Figure 7 shows the result of the inversion, in which vertical bars denote the uncertainties at each position that, as is shown and already known, grow toward the interior. The result is in complete agreement with previous determinations down to about 0.5 $R_\odot$ (Thompson et al. 1996; Tomczyk et al. 1995a). The sharp decrease at the base of the convection zone is clearly seen followed by a plateau (with a very small bump) down to approximately 0.45 $R_\odot$. Here we do not see a local maximum at approximately 0.4 $R_\odot$ that Tomczyk et al. (1995a) find, but we do agree on the sudden drop again down to approximately 0.3 $R_\odot$; from here downward it seems to reach a "plateau" at approximately 400 nHz. Therefore, from the inversion of these measurements it seems that a fraction of the solar radiative interior rotates at a rate slower than that of the surface.

Although the rotation rate could increase even at inner portions of the solar core, these measurements confirm earlier findings (Duvall et al. 1984; Tomczyk et al. 1995a)

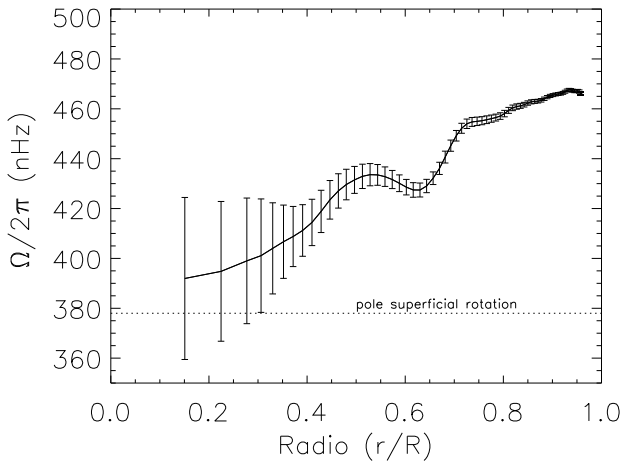

FIG. 7.—Solar equatorial rotation rate as a function of depth

and provide strong arguments against theories of stellar structure that predict large gradients in the solar angular momentum transport at the core boundary (Pinsonneault et al. 1989). A way out of this could be if the core were magnetically connected with the poles or high-latitude regions of the Sun, which rotate much slower than the equator. Another possibility could be the existence of a core rotating faster, but around an axis inclined with respect to the one seen at the surface. In this sense, a magnetized solar core could interact with rotation, causing changes in its rotation rate that could explain even the large scatter in the splitting of $l = 1$ modes (Appourchaux et al. 1995a).

At this deep into the Sun's core, there really are not enough data from low-l modes to be able to draw firm conclusions. Even if the splitting found for $l = 1$ modes (e.g., Elsworth et al. 1995; Lazrek et al. 1996) is included, not much change is found. Not even an improvement in the accuracy of the frequency determinations will dramatically change these views, considering that there is little room for improvement on this, as the precision of our frequency measurements is consistent with the limits imposed by the random nature of excitation and damping of the modes. In our opinion, only g-mode frequencies have the potential to cast new light into this rather poorly known solar core rotation rate. These are the expectations on the LOI instrument on board VIRGO, which could, in principle, be able to measure such otherwise elusive modes.

We are deeply indebted to all members of the IAC Helioseismology team for help with the observations and useful discussions. We are also thankful to S. Tomczyk and J. Schou for sending the LOWL results of their analysis. This work utilizes data obtained by the Global Oscillations Network Group (GONG) project, managed by the National Solar Observatory, a Division of the National Astronomy Observatories, which is operated by AURA, Inc., under cooperative agreement with the National Science Foundation. The data were acquired by instruments operated at Big Bear Solar Observatory, High Altitude Observatory, Learmonth Solar Observatory, Udaipur Solar Observatory, Instituto de Astrofísica de Canarias, and Cerro Tololo Inter-American Observatory. This work has been made possible thanks to the financial support of the Spanish CICYT under grants ESP-90-0969, ESP-91-1441, and PB91-0530. M. C. R. S. is also thankful for financial support received from the Brazilian Institution, CNPq (202504/91-3).

REFERENCES

Andersen, B. N., Domingo, V., Jones, A. R., Jiménez, A., Pallé, P. L., Régulo, C., & Roca Cortés, T. 1988, in Seismology of the Sun and Sun-like Stars, ed. E. J. Rolfe (ESA SP-286), 385
Anderson, E. R., Duvall, T. L., Jr., & Jefferies, S. M. 1990, ApJ, 364, 699
Anguera Gubau, M., Pallé, P. L., Pérez Hernández, F., Régulo, C., & Roca Cortés, T. 1992, A&A, 255, 372
Appourchaux, T., & Andersen, B. N. 1990, Sol. Phys., 128, 91
Appourchaux, T., Toutain, T., Jiménez, A., Rabello Soares, M. C., Andersen, B. N., & Jones, A. R. 1995a, in Proc. 4th SOHO Workshop: Helioseismology, ed. J. T. Hoeksema, V. Domingo, B. Fleck, & B. Battrick (ESA SP-376[2]), 265
Appourchaux, T., Telljohann, U., Martin, D., Fleur, J., & Lévêque, S. 1995b, in Proc. 4th SOHO Workshop: Helioseismology, ed. J. T. Hoeksema, V. Domingo, B. Fleck, & B. Battrick (ESA SP-376[2]), 359
Appourchaux, T., Toutain, T., Telljohann, U., Jiménez, A., Rabello Soares, M. C., Andersen, B. N., & Jones, A. R. 1995c, A&A, 294, L13
Brown, T. M. 1985, Nature, 317, 591
———. 1986, in Seismology of the Sun and the Distant Stars, ed. D. O. Gough (Dordrecht: Reidel), 199
Brown, T. M., et al. 1989, ApJ, 343, 526
Chaplin, W. J., et al. 1995, in Proc. 4th SOHO Workshop: Helioseismology, ed. J. T. Hoeksema, V. Domingo, B. Fleck, & B. Battrick (ESA SP-376[2]), 391
Christensen-Dalsgaard, J. 1984, JPL Publ. 84-84, 219
Claverie, A., Isaak, G. R., McLeod, C. P., & van der Raay, H. G. 1979, Nature, 282, 591
Claverie, A., Isaak, G. R., McLeod, C. P., van der Raay, H. G., & Roca Cortés, T. 1981, Nature, 293, 443
Cuypers, J. 1980, A&A, 89, 207
Deubner, F. L. 1975, A&A, 44, 371
Deubner, F. L., Ulrich, R. K., & Rhodes, E. J., Jr. 1979, A&A, 72, 177
Duvall, T. L., Jr., Dziembowski, W. A., Goode, P. R., Gough, D. O., Harvey, J. W., & Leibacher, J. W. 1984, Nature, 310, 22
Duvall, T. L., Jr., & Harvey, J. W. 1983, Nature, 302, 24
———. 1984, Nature, 310, 19
Duvall, T. L., Jr., Harvey, J. W., & Pomerantz, M. A. 1986, Nature, 321, 500
Edmonds, A. R. 1960, Angular Momentum in Quantum Mechanics (Princeton: Princeton Univ. Press)
Elsworth, Y., et al. 1990, MNRAS, 242, 135
———. 1995, Nature, 376, 669
Eff-Darwich, A. 1996, Ph.D. thesis, Univ. La Laguna, Tenerife
Eff-Darwich, A., & Pérez-Hernández, F. 1996, A&A, in press
Fröhlich, C., et al. 1995, Sol. Phys., 162, 101
Gough, D. 1981, MNRAS, 196, 731
Grec, G., Fossat, E., & Pomerantz, M. 1980, Nature, 288, 541
Hill, F., et al. 1996, Science, 272, 1292
Jiménez, A., et al. 1994, ApJ, 435, 874
Lazrek, M., et al. 1996, Sol. Phys., in press
Libbrecht, K. G., & Morrow, C. A. 1991, in Solar Interior and its Atmosphere, ed. A. N. Cox, W. C. Livingston, & M. S. Matthews (Tucson: Univ. Arizona Press), 479
Libbrecht, K. G. 1988, ApJ, 334, 510
———. 1989, ApJ, 336, 1092
Loudagh, S., et al. 1993, A&A, 275, L25
Morrow, C. A. 1988, in Seismology of the Sun and Sun-like Stars, ed. E. Rolfe (ESA SP-286), 137
Pallé, P. L., Pérez Hernández, F., Régulo, C., & Roca Cortés, T. 1988, in Seismology of the Sun and Sun-like Stars, ed. E. Rolfe (ESA SP-286), 125
Pinsonneault, M. H., Kawaler, S. D., Sofia, S., & Demarque, P. 1989, ApJ, 338, 424
Rabello Soares, M. C. 1996, Ph.D. thesis, Univ. La Laguna, Tenerife
Rabello Soares, M. C., et al. 1996, A&A, in press
Régulo, C., Jiménez, A., Pallé, P. L., Pérez Hernández, F., & Roca Cortés, T. 1994, ApJ, 434, 384
Ritzwoller, M. H., & Lavely, E. M. 1991, ApJ, 369, 557
Thompson, M. J., et al. 1996, Science, 272, 1300
Tomczyk, S., Schou, J., & Thompson, M. J. 1995a, ApJ, 448, L57
Tomczyk, S., Streander, K., Card, G., Elmore, D., Hull, H., & Cacciani, A. 1995b, Sol. Phys., 159, 1
Toutain, T., & Fröhlich, C. 1992, A&A, 257, 287